EDGE AND COUPLED CORE/EDGE TRANSPORT MODELLING IN TOKAMAKS*

L.L. LODESTRO, T.A. CASPER, R.H. COHEN, N. MATTOR,
L.D. PEARLSTEIN, G.D. PORTER, M.E. RENSINK, T.D. ROGNLIEN,
D.D. RYUTOV, H.A. SCOTT, and A.S. WAN
Lawrence Livermore National Laboratory
P. O. Box 808, Livermore, CA 94551, USA

Abstract

Recent advances in the theory and modelling of tokamak edge, scrape-off-layer (SOL) and divertor plasmas are described. The effects of the poloidal $E\times B$ drift on inner/outer divertor-plate asymmetries within a 1D analysis are shown to be in good agreement with experimental trends; above a critical $\mathbf{v}_{E\times B}$, the model predicts transitions to supersonic SOL flow at the inboard midplane. 2D simulations show the importance of $E\times B$ flow in the private-flux region and of ∇B-drifts. A theory of rough plasma-facing surfaces is given, predicting modifications to the SOL plasma. The parametric dependence of detached-plasma states in slab geometry has been explored; with sufficient pumping, the location of the ionization front can be controlled; otherwise only fronts near the plate or the X-point are stable. Studies with a more accurate Monte-Carlo neutrals model and a detailed non-LTE radiation-transport code indicate various effects are important for quantitative modelling. Detailed simulations of the DIII-D core and edge are presented; impurity and plasma flow are discussed and shown to be well modelled with UEDGE.

1. INTRODUCTION

Comprehensive modelling of the scrape-off-layer (SOL) plasma in a tokamak is a central issue for the design of high-power machines. The SOL's importance lies in its roles in plasma/wall interactions, impurity and ash control, and interactions with the edge plasma (the outer-most closed flux-surfaces). Here we describe theory and simulation advances in modelling edge/SOL plasmas and make detailed comparisons with recent measurements in DIII-D. We present enhanced-performance core-transport scenarios for DIII-D, for which edge conditions and modelling are particularly important, and report the results of self-consistently coupled core/edge calculations.

2. PARTICLE-DRIFT EFFECTS IN THE EDGE AND SOL

2.1. In/out divertor-plate asymmetries produced by the $E\times B$ drift: 1D model

It is seen experimentally that reversing the toroidal magnetic field $B_{\rm tor}$ can considerably affect the distribution of particle and heat fluxes to the inner and outer divertor plates [1]. A possible cause is the poloidal $E\times B$ drift induced by the outward radial electric field that is always present in the SOL, arising from the sheath conditions at the divertor plates and the decrease of T_e with distance from the separatrix. The drift is towards the outer plate for the "normal" orientation of $B_{\rm tor}$ (ion ∇B-drift directed towards the plates), and changes sign with the reversal of $B_{\rm tor}$. It is therefore tempting to attribute experimental trends to this drift, and the observed trends in the heat-flux asymmetry do correlate well with its direction. However, analysis of SOL particle fluxes for a uniform B [2] has shown that the density and pressure asymmetries apparently anti-correlate with experiment. Here, with a more realistic model, we find agreement with experimental trends even in 1D. An important point of our analysis is that the cross-section of the flux tube connecting the two divertor plates is minimum on the inner-most side of the magnetic surface, thereby creating the geometry of a Laval nozzle for the plasma flow on its way to the inner strike-point [3]. This leads to the possibility of supersonic flow [2]. The second component of a more realistic picture is the difference in T_e at the two plates caused by the much larger surface area of the outer cf. inner part of the last closed flux-surface. Due to this, even in the absence of drifts the heat flux to the outer strike-point must exceed that to the inner strike-point [4]. With a poloidal drift imposed on such a plasma flow, all experimentally observed correlations are recovered. Figure 2.1 illustrates the in/out density asymmetry vs. poloidal $\mathbf{v}_{E\times B}$ for strike-point temperature asymmetries $T_{\rm in}/T_{\rm out} = 1$ and 0.16, and mirror ratio along the flux-tube $R = 1.5$. On the left branches of the curves, the plasma flow is supersonic between the inboard midplane and inner strike-point. Radial drift-effects (included in the 2D treatment below) also give the experimentally observed correlations [5]. We emphasize that poloidal drifts are at least as important.

* Work performed for USDOE under contract W-7405-ENG-48 at LLNL.

2.2. 2D drift effects using the UEDGE code

For full 2D modeling of the edge and SOL we evolve n_{gas}, the plasma densities, T_e, T_i, plasma potential ϕ, and ion and neutral parallel velocities with UEDGE [6]. A new element is the inclusion of both anomalous viscosity and classical ∇B drifts in the charge-continuity equation. The anomalous radial current is obtained within a consistent ordering of the classical transport equations, using an enhanced collisionality to model turbulence while maintaining all intrinsic symmetries. Alternatively, toroidal turbulent transport equations are derived, with quasilinear closures for the anomalous terms. Both models give a 4^{th}-order radial differential equation for ϕ which can be used both inside the separatrix, where radial force balance is crucial, and outside, where parallel currents dominate. ∇B drifts also contribute significantly to the current, while the current from charge-exchange near the separatrix is typically small for DIII-D parameters. The resulting E_r is shown in Fig. 2.2. Except near the separatrix, the poloidal variation comes mainly from the changing distance between flux surfaces with nearly constant ϕ; for this lower single-null DIII-D configuration, the presence of a 2^{nd} X-point near the top of the plasma produces a local minimum in E_r there. Note the large shear near the separatrix, which should help stabilize edge/SOL turbulence. In addition to the poloidal $\mathbf{v}_{E\times B}$ in the SOL addressed in the 1D model above, we find significant $\mathbf{v}_{E\times B}$ flows under the X-point in the private flux region. This flow enhances [decreases] the inner plate density for normal [reversed] B_{tor}. The gas-puff rate required for inner-leg detachment is then lower for normal B_{tor}, in agreement with Alcator C-Mod [1] and DIII-D observations. Also, the change in plate current-profile with normal cf. reversed B_{tor} obtained from probe measurements on JET [7] is qualitatively reproduced by our calculations.

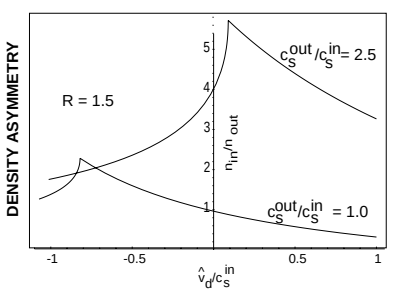

Fig. 2.1. Poloidal asymmetry in divertor-plate density vs. normalized poloidal $\mathbf{v}_{E\times B}$.

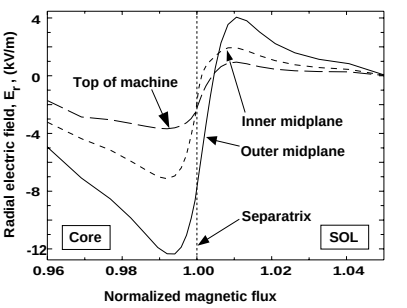

Fig. 2.2. UEDGE-*computed* E_r *at 3 poloidal cuts for a low-power* DIII-D *case with* $\mathbf{v}_{i\nabla B}$ *toward the X-pt.*

3. SHEATH OVER A SURFACE WITH SMALL-SCALE IMPERFECTIONS

A divertor-plate surface typically has fine "topographic" structure determined by the intrinsic properties of the material (e.g., the grainy structure of graphite) and by erosion. Their characteristic size can vary broadly. The magnetic field intersects the plate at a shallow angle α. We show that the presence of fine surface structures, together with the smallness of α, gives rise to many interesting new phenomena in the sheath. We assume the surface is formed by randomly distributed cones of height h, with base radius and distance between neighboring cones also $\sim h$. We first assume that the electric field does not significantly affect the particle motion, and then consider complications. We find that, at small α's, the plasma stream is entirely absorbed near the tops of the cones, so that the fraction of the rough surface "wetted" by plasma particles is small, resulting in local heat and particle fluxes near the tips of the cones much higher than for a flat divertor plate. Using general scaling arguments [8], we find expressions for the wetted fraction as a function of two parameters, α and ρ_i/h. In a number of cases, the electrons wet a much smaller fraction than the ions. Then, to achieve quasineutrality, potentials will be formed to prevent the ions from entering the zones inaccessible to electrons. Projecting along $\mathbf{B}$ into the bulk plasma, this fine potential structure will cause additional diffusion towards the walls. In quasi-steady-state, a gradual ionization of neutrals will create a cold-plasma neutralizing background, restoring the original picture with different fractions of the surface wetted by SOL electrons and ions.

4. DETACHED PLASMA STATES; MONTE-CARLO NEUTRALS; RADIATION EFFECTS

There is evidence [9] as well as a recent simple theory [10] raising concern that a fully detached plasma evolves to an X-point MARFE with degraded core confinement. We use UEDGE to

generate a map of stationary solutions vs. parameters (core n_e, input power to the SOL, and particle pumping at the divertor plate and side-walls) in a slab geometry simulating half a single-null divertor configuration. We find that when the divertor side-walls are pumping surfaces, solutions for all core plasma densities and powers are stable. For no pumping, stable thermally attached plasma solutions exist above some minimum input power as shown in Fig. 4.1. For lower power, three solutions exist, with the ionization front close to the plate, midway to the X-point and close to the X-point. The middle solution is temporally unstable; the other two are stable. At even lower power, only one solution exists; it is stable and approaching a MARFE-like state.

To assess the inertial fluid-neutrals model [11] in UEDGE, we compare to coupled UEDGE/Monte-Carlo (M-C) neutrals [12] calculations. With pumping at the side-walls and divertor plate, the two models qualitatively agree for both attached and detached states. However, without pumping no stable states have been found with M-C neutrals (cf. Fig. 4.1). This difference may be due to lack of strict particle balance in the coupled codes, or to molecules, the dominant species in the detached region for the M-C model but not present in our fluid-neutrals model. For a given plasma profile, the atomic density from the latter far exceeds the M-C molecular density because recycling atoms must diffuse upstream from the divertor plate via charge-exchange while molecules are nearly collisionless in the cold detached region. As a result, the transfer of momentum and energy to the neutrals via charge-exchange is significantly reduced in the M-C model.

Radiation transport is investigated using the CRETIN code with UEDGE plasma profiles. Simulated low-power detached operation with pure hydrogen in DIII-D shows a reduction by a factor ~ 50–100 in the hydrogen radiation at the plate and side-walls. Also, the Lyman-series flux to a simulated detector is strongly distorted, indicating the need for detailed detector modelling.

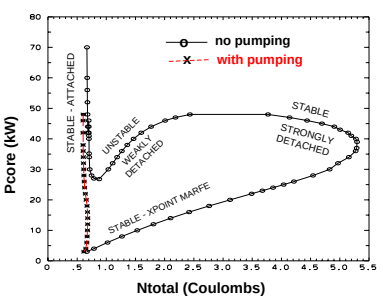

Fig. 4.1. Stationary UEDGE *solutions with & without pumping. Input power to the* SOL *is Pcore; total particle inventory (ions+neutrals) is Ntotal; ion density at the innermost core surface is fixed at* $7 \times 10^{19}/\mathrm{m}^3$.

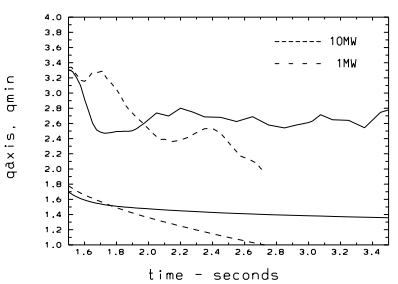

Fig. 5.2. Temporal variation of q_{axis} *and* q_{min} *for ECH powers of 1 & 10 MW with* q_{min} *sustained for 25* τ_{E} *at 10 MW as simulated by* CORSICA.

5. PROGRESS AND DIRECTIONS IN DIII-D SIMULATIONS

5.1. Modelling the DIII-D edge and SOL with UEDGE

UEDGE has been validated against a large variety of data from DIII-D, including radial profiles of n_e, T_e, and T_i at the outer midplane, 2D plasma profiles in the divertor region, bolometric measurements of the total radiation profiles, and profile measurements of D_α emission [9,13]. Recent code improvements include realistic models for both chemical and physical sputtering [14]. Two diagnostics are useful for validating these models: the bolometric measurement of total radiated power and measurement of the parallel flow velocity of both impurity and primary ions [15,16]. Impurity radiation patterns are determined by a combination of the carbon source distribution and the radial and parallel transport of each of its ionization states, together with detailed atomic physics. We assume anomalous radial diffusion in UEDGE, and use a spatially constant diffusivity for all ion species. We find the dominant terms in the impurity-ion parallel force-balance to be drag on the hydrogenic fuel ions and thermal forces which move the impurities up ∇T_i. The parallel velocities of both the fuel and C^+ ions predicted by the UEDGE model are consistent with measurements, as shown in Fig. 5.1. We compare the simulated and measured Mach number of the primary ion flow measured along a vertical line just outside the outer strike point in (a), and the parallel C^+ velocity along a line which views the plasma tangential to a surface lying just outside the X-point in (b). The C^+ velocity is measured spectroscopically, permitting determination of $\pm$ flow components at different radii. Similar agreement is obtained for a detached outer leg, and for a discharge shifted radially outward enabling diagnosis of the inner leg.

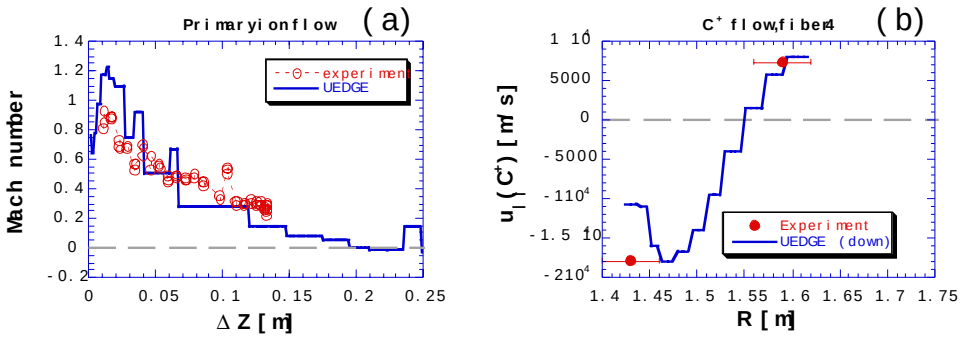

Fig. 5.1. Comparsion of simulated and measured flows for the primary ions (a) and singly ionized carbon (b) in DIII-D. *Positive flow is toward the outer plate.*

We also investigate impurity transport from the walls of DIII-D to the core. Typically we find buildup of C^{+4} at a force null (with forces pointing towards the null). The null position(s) are determined by details of the parallel T_i and fuel-ion-flow patterns. The C^{+4} density builds up to a high level in the SOL, then diffuses into the core where it is quickly ionized to higher states.

5.2. High-performance DIII-D modelling with Corsica

A combination of heating and current drive during Ohmic ramp-up leads to the formation of discharges with negative central shear (NCS) and high performance in many machines. To extend their performance to long pulse-lengths and ultimately steady-state requires active control of heating, fueling and current-drive systems. We are modelling the effects of ECH and ECCD in DIII-D for this purpose and to broaden the NCS region. Time-dependent CORSICA 1 simulations using a transport model which ties the location of the barrier to $q_{\min}$ indicate that at powers > few MW absorbed, the barrier can be sustained for several τ_E, as shown in Fig. 5.2, where the position of $q_{\min}$ was maintained for $\sim 25\ \tau_E$. Edge profile conditions are critical in these regimes. In L-mode, central pressure-peaking can cause disruptions, whereas H-mode profiles reduce beam penetration and support steep edge gradients which drive currents resulting in ELMS. In many of the DIII-D experiments, the pressure profile is controlled by biasing the plasma position, inducing L/H transitions. To assess our ability to control profiles and to analyse the interplay of edge physics and core confinement, LLNL's CORSICA 2 code [18] is being extended and validated against DIII-D. CORSICA 2 couples core transport to UEDGE in a fully self-consistent manner, such that UEDGE can be run either time-dependently or in quasi-static equilibrium with the shared boundary conditions at the outer core. Coupled fields include n_D, n_α, T_e, T_i, n_{gas}, and toroidal momentum. With the addition of SOL-turbulence-driven transport coefficients [19] to UEDGE, we have simulated an L/H transition in DIII-D, with profiles in qualitative agreement with experiment.

References

[1] HUTCHINSON, I.H., et al., Plasma Phys. and Contr. Fusion **37** (1995) 1389.
[2] COHEN, R.H., RYUTOV, D.D., Comm. on Plasma Phys. and Contr. Fus **16** (1995) 255.
[3] RYUTOV, D.D., Contrib. Plasma Phys. **36** (1996) 207.
[4] HARBOUR, P.J. et al., Contrib. Plasma Phys. **28** (1988) 417.
[5] STANGEBY, P.C., CHANKIN, A.V., Nucl. Fusion, **36** (1998) 839.
[6] ROGNLIEN, T.D., BROWN, P.N., et al., Contrib. Plasma Phys **34** (1994) 362.
[7] SCHAFFER, M.J., CHANKIN, A.V, GUO, H.Y., et al., Nucl. Fusion **37** (1997) 83.
[8] COHEN, R.H., et al., J. Nucl. Materials, to be published.
[9] PORTER, G.D., ALLEN, S.L., BROWN, M., et al., Phys. Plasmas **3**(5) (1996) 1967.
[10] KRASHENINNIKOV, S.I., RENSINK, M., et al., J. Nucl. Materials, to be pub., 1999.
[11] WISING, F., KNOLL, D.A., et al., Contrib. Plasma Phys **36** (1996) 309.
[12] REITER, D., J. Nucl. Mat. **196–198** (1992) 80.
[13] FENSTERMACHER, M.E., ALLEN, S.L., et al., Phys. Plasmas **4**(5) (1997) 1761.
[14] DAVIS, J.W., and HAASZ, A.A., J. Nucl. Mater. **241–243** (1997) 37–51.
[15] ISLER, R.C., BROOKS, N.H., WEST, W.P., et al., submitted to Phys. Plasmas (1998).
[16] BOEDO, J., PORTER, G.D., SCHAFFER, M., et al., accepted by Phys. Plasmas (1998).
[17] CASPER, T.A., et al., Proc. 25th EPS Conf. Contr. Fus. and Plasma Phys., Prague (1998).
[18] TARDITI, A., et al., Contrib. Plasma Phys. **36** (1996) 132.
[19] COHEN, R.H., and XU, X.Q., Phys. Plasmas **2** (1995) 3374.